THE EFFECTS OF ALKALINE REAGENT AND SYNTHESIS ATMOSPHERE ON THE CHEMICAL, MORPHOLOGICAL, AND MAGNETIC CHARACTERISTICS OF MAGNETITE NANOPARTICLES FOR HYPERTHERMIA TREATMENT

[1]ZIBA HEDAYATNASAB, [2]ALI DABBAGH, [3]FAISAL ABNISA, [4]HAMID REZA MADAAH HOSSEINI, [5]NOOR HAYATY ABU KASIM, [6]NOORSAADAH ABDULRAHMAN, [7]WAN MOHD ASHRI WAN DAUD

[1,3,7]Department of Chemical Engineering, Faculty of Engineering, University of Malaya,
[2]School of Medicine, Faculty of Health and Medical Sciences, Taylor's University,
[2,4]Department of Materials Science and Engineering, Sharif University of Technology,
[5]Wellness Research Cluster, Institute of Research Management & Services, University of Malaya,
[6]Department of Chemistry, Faculty of Science, University of Malaya
E-mail: [1]Z_hedayatnasab@yahoo.com, [2]ali.dabbagh@taylors.edu.my, [3]faisal.abnisa@gmail.com, [4]madaah@sharif.edu, [5]nhayaty@um.edu.my, [6]noorsaadah@um.edu.my, [7]ashri@um.edu.my

Abstract - This study investigated the simultaneous effects of two alkaline reagents including sodium hydroxide (NaOH) and ammonium hydroxide (NH4OH) as well as the aerobic and anaerobic (N_2) atmospheres on the crystalline structure, zeta potential, aggregation vulnerability, magnetic characteristics, heating efficiency of iron oxide nanoparticles (IONPs) under hyperthermia condition. The obtained results indicated the crucial impact of the synthesis atmosphere on the crystalline structure and magnetic properties, while the alkaline reagent type mainly governed the zeta potential and particle morphology. Although the IONPs precipitated with NaOH under anaerobic environment exhibited higher zeta potential and thus slightly less aggregation vulnerability, those synthesized using NH_4OH in anaerobic atmosphere provided enhanced crystallinity and magnetic properties. Therefore, due to the negligible effect of alkaline reagent type on the morphological characteristics of the nanoparticles, an anaerobic atmosphere with NH_4OH as the precipitating agent was chosen as the optimal synthesis condition, resulting in particles with higher crystallinity and enhanced superparamagnetic properties. The temperature control in the secure range of magnetic hyperthermia therapy (MHT) was achieved by the variation of either the IONPs concentration in the aqueous solution or the field strength. The heating capability of the IONPs was also quantified by the specific absorption rate (SAR), and the intrinsic loss parameter (ILP). The SAR and ILP values were positively influenced by the field strength, while increase of the particles concentration resulted in reduced SAR and ILP, probably due to the reduced dominance of the heating loss mechanism. The IONPs with the lowest concentration of 1 $mg.ml^{-1}$ and 14 nm crystalline size expressed the highest SAR value of 316.43 $W.gFe^{-1}$..

Index Terms - Alkaline Reagent, Iron Oxide Nanoparticles, Magnetic Hyperthermia Therapy, Synthesis Atmosphere.

I. INTRODUCTION

Iron oxide nanoparticles (IONPs) have been at the forefront of nanotechnology research due to their unparalleled and superior properties including high magnetization, biocompatibility, facile synthesis, and low cost which make them highly appropriate for various biomedical applications including magnetic hyperthermia therapy (MHT) [1, 2]. Hyperthermia therapy is a stated clinical protocol in oncology, which attempts to destroy the cancerous cells via boosting the tumor temperature from the physiological level (37°C) to temperature range of 42-47 °C, as such cells are more sensitive to high temperatures than normal cells due to their immature structure. The temperature rise in the intracellular medium is often achieved using IONPs as therapeutic agents and external alternating magnetic field (AMF) [3].

The capability of IONPs in heat generation from the magnetic coupling between their magnetic moments and the applied AMF is determined using a caloric parameter known as the specific absorption rate (SAR), which is the induction heating power absorbed per unit mass of the magnetic NPs. This value is governed by various parameters such as the particle composition, size, shape, concentration, as well as strength and frequency of AMF [4]. As the particles concentration must be minimized to prevent potential disorders for the treated patients, the experimental conditions applied for the synthesis of the NPs play vital role in not only produce IONPs with high SAR value but also provide a safe heating therapy [5, 6].

IONPs are comparatively instable in aerobic condition derived from their significant vulnerability to oxidation by low amounts of oxygen present in the environment, leading to lose of dispersibility and magnetism. Therefore, provision of an anaerobic condition via injection of inert gases is considered as a requisite to prevent IONPs activity towards the environmental oxygen [7]. The pH of the synthesis solution is the second decisive factor which plays a pivotal role in particles dispersibility. The stability of IONP suspensions in aqueous solutions can be controlled by altering the pH values through dilution of the alkaline reagent or incorporation of varied alkaline solutions [8, 9]. Ammonium hydroxide

(NH_4OH) and sodium hydroxide (NaOH) are the most widely used precipitating agents for synthesis of IONPs, which could provide maximum pH values of 10-11 and 12-13, respectively [10]. The differed pH values obtained by these alkalis could potentially affect various chemical, physical, morphological, and magnetic characteristics of the resulting particles as well as their aggregation vulnerability.

In spite of the crucial impacts of synthesis atmosphere and precipitating reagent, the comparative studies on significance of their effects on different properties of the resultant IONPs are scarce. In fact, determination of the main governing parameter of various properties requires quantitative investigations and comparative analyses of these properties at different experimental conditions. Thereby, this study aimed to investigate the simultaneous effects of two environmental conditions including aerobic and anaerobic atmosphere as well as two popular precipitating agents including NaOH and NH_4OH on the chemical, physical, morphological, and also magnetic properties of IONPs synthesized without using any stabilizing compound. The synthesized IONPs were also exposed to the external AMF at varied field amplitudes to evaluate their effectiveness as heating agents in MHT. Therefore, the present study could aid in appropriate selection of the experimental parameters to synthesize nanoparticles with desired properties according to their intended application.

II. MATERIALS AND METHODS

A. Materials

Ferric chloride hexahydrate (FeCl3.6H2O>99%), Ferrous chloride (FeCl2.4H2O>99%), NaOH pellets (99%), NH4OH (28%w/w) and ethanol were purchased from R&M Chemicals and used without further purification or modification as the starting materials for synthesis of IONPs.

B. Synthesis of IONPs

IONPs were synthesized in two different environmental conditions using two varied alkaline solutions for precipitation of four types of IONPs as follows: aerobic condition with NaOH (NaOH.Air, IO_4), aerobic condition with NH_4OH (NH_4OH.Air, IO_2), anaerobic condition with NaOH ($NaOH.N_2$, IO_3) and anaerobic condition with NH_4OH ($NH_4OH.N_2$, IO_1). In a typical procedure, $FeCl_3.6H_2O$ (2.33 g, dissolved in 8 mL distilled water) and $FeCl_2 \cdot 4H_2O$ (0.85 g, dissolved in 2 mL distilled water) were volumed up to 50 mL by distilled water, and then 50 mL of either NH_4OH or NaOH solutions was added dropwise under vigorous stirring. After an hour, the synthesized nanoparticles were separated using a small magnet, washed once with ethanol, and five times with distilled water to remove impurities. The particles were then dried at 80 °C for 24 hours for further analyses.

C. Characterization of IONPs

The zeta potential values of IONPs were quantified using a Zetasizer instrument (Nano ZSP instrument, Malvern Instruments, Worcestershire, UK), while their phase structure and crystallinity were investigated by powder X-ray diffraction (XRD; Philips PW1840, Amsterdam, the Netherlands) equipped with Cu-Kα radiation (λ=1.542 A°) at 2θ angle of 10° to 80°. The full width at half maximum (B) as an indicator of the crystallinity degree was measured using Origin Pro software (version 9.4, Origin Lab, Hampton, MA). Then, the crystallite sizes of four different samples were calculated according to the Debye Scherer's formula [11]:

$$D = \frac{K\lambda}{B\cos(\theta)} \quad (1)$$

where D represents the crystallite size and K is 0.94.

The structural morphologies of IONPs were observed using transmission electron microscopy (TEM; LEO Libra 120 kV, Carl Zeiss AG, Germany) and the mean particle size of each group was examined using ImageJ software by measuring at least 100 randomly selected nanoparticles. Magnetic characterization of the samples was carried out using a vibrating-sample magnetometer (VSM; model 7400 series, Lakeshore, Chicago, IL) at ambient temperature. The magnetic hysteresis loops were measured in the field range from 0 to ± 8 × 10^3 G (0.8 T).

D. Magnetic Hyperthermia Studies

To study the impact of colloidal IONPs dispersion properties on the magnetic hyperthermia properties, synthesized nanoparticles with varied concentration from 1mg ml^{-1} to 5mg ml^{-1} were dispersed in aqueous media, i.e., distilled water in accordance with the structure of the human body that is made up about 70% water. The induction heating efficiency of the colloidal magnetic nanoparticles was determined by subjecting the aqueous IONPs towards the external AMF with six varied electric currents (50-300 A). For this purpose, magnetic hyperthermia experiment of IONPs was carried out in plastic micro centrifuge tube (2 ml) placed in the center of helical coil with inner diameter of 2.54 cm and 8 turns of an induction heating machine (Easy Heat 8310, Ambrell, UK) with the frequencies that

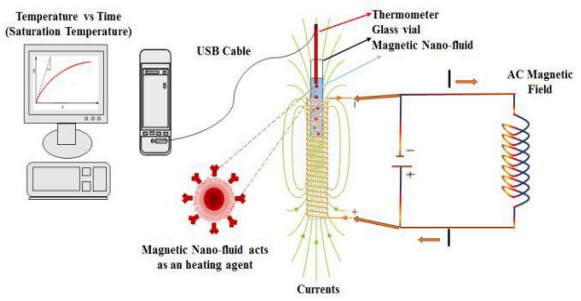


Fig. 1. The schematic of the experimental setup for MHT [7].

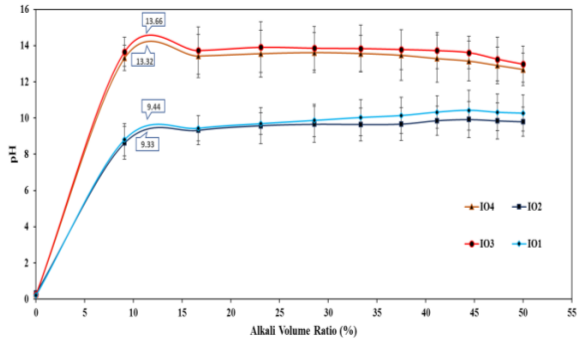


Fig. 2. The rate of pH rises during dropwise addition of precipitating agents under different synthesis atmospheres.

corresponded to the applied currents using the provision of water circulation coils to keep the coil temperature at room temperature. The schematic of the experimental setup utilized for this present MHT is illustrated in Fig.1. For the conducted hyperthermic experiments, the magnetic field (H) was calculated from the following relationship [12-14]:

$$H(Oe) = 1.257\frac{ni}{L} \qquad (2)$$

where n, i, and L indicate the coil turns, applied current (A), and coil diameter (cm), respectively. The calculated magnetic field values at six applied currents, were 197.85, 395.82, 593.80, 791.78, 989.76 and 1187.61 Oe (equivalent to 15.74, 31.49, 47.24, 62.99, 78.74 and 94.48 $kA.m^{-1}$), respectively. Thereby, varied experimental conditions were conducted to determine the optimal IONPs concentration as well as AMF amplitude strength. The hyperthermia temperatures (T_H) profiles were recorded during the exposure of the IONPs to the AMF over 90 min.

E. Specific Absorption Rate Determination

The heating efficiency of IONPs quantitatively evaluated through SAR in the presence of an external AMF. The SAR values are actually calculated using the following empirical formula [15]:

$$SAR\ (W.g^{-1}) = (\frac{C_m}{x})(\frac{dT}{dt})_{t\to 0} \qquad (3)$$

where C_m is the specific heat capacity of the colloidal solution which is the combination of both IONPs weight and medium weight; however, IONPs weight is negligible because of low concentrations, thus only specific heat capacity of medium, "water" is contributed with value of 4.18 J $g^{-1}.K^{-1}$. The value of x is indicated the ratio between the medium and IONPs weights and dT/dt is the initial slope of the time-dependent temperature curve which in present study, time considered up to 1 min to calculate the slope. Thereby, SAR values are calculated from the linear portion of the induction heating curves which alter rather narrowly.

SAR values should be as high as possible to minimize the amount of IONPs applied for MHT for not only better inductive heating performance but also preventing eddy currents which cause unpredictable disorders for human body in clinical trials. As a matter of the fact, the induction heating of IONPs is originated from their power loss in the AMF consequently, the induction heating power relies on magnetic fields parameter, amplitude (H) as well as frequency (f) with considering a human tolerable range of these parameters [7, 16]. The intrinsic loss power (ILP) defines as a heating transformation capability which is used to standardize and normalize the SAR values with respect to magnetic field amplitude (H) and frequency (f) and is calculated from the following equation [17, 18]:

$$ILP\ (nH.m^2.kg^{-1}) = \frac{SAR}{H^2.f} \qquad (4)$$

All reported SAR values were calculated by more than triplicate experimental measurements. Data are presented as means and ± standard deviations of the mean.

III. RESULTS AND DISCUSSION

The rate of pH rise during dropwise addition of the alkaline solutions into the reaction chamber containing $FeCl_3.6H_2O$ and $FeCl_2{\cdot}4H_2O$ as iron precursors is shown in Fig.2. Addition of the iron precursors to the aqueous solution resulted in drastic pH reduction to approximately zero due to the strong acidity of the precursors. By dropwise addition of the alkaline solutions into the iron mixture, pH rose moderately while further injection of 5ml led to rapid pH increases to above 10 and 13 for the NH_4OH and NaOH, respectively and then no significant increase in the solution pH was observed by increasing the volumetric ratios of the alkalis. However, continued dropwise addition of the alkaline reagent was necessary to supply sufficient OH^- ions for precipitation of the entire Fe^{2+} and Fe^{3+} [19]. Consequently as shown in Fig.3, the zeta potential values of the magnetic samples synthesized in NaOH (-36.6 mv and -39.2 mv for IO_4 and IO_3 respectively) were significantly higher than those of the particles produced in NH_4OH (-15.8 mv and -19.2 mv for IO_2 and IO_1), which could potentially lead to their relatively higher stability and lower aggregation in aqueous solutions. Besides, the pH values of the synthesis solutions under atmosphere were lower than their counterparts under N_2 atmosphere, probably due to the increased oxidation vulnerability of the nanoparticles in presence of CO_2, resulting in higher acidity of IONPs followed by lower zeta potential values [20]. Moreover, lower pH values obtained by the mild alkali may contribute to lower rates of particle formation and smaller particle sizes of IO_1 and IO_2. It is noteworthy that flow of nitrogen gas assists the effect of NH_4OH in the reduction of

particle size as well as preventing oxidation leading to sufficient surface stability against agglomeration [21]. The XRD spectra of the IONPs synthesized using NaOH or NH_4OH in either aerobic or anaerobic atmospheres (Fig.4) confirmed formation of magnetite phase with the space group of $Fd3^{-}m$, (JCPDS 00-001-1111) where the peaks observed at 2θ values of 30°, 35°, 43°, 54°, 57°, and 63° respectively corresponded to (220), (311), (400), (422), (511), and (440) family planes (PDF 89–4319) inthe

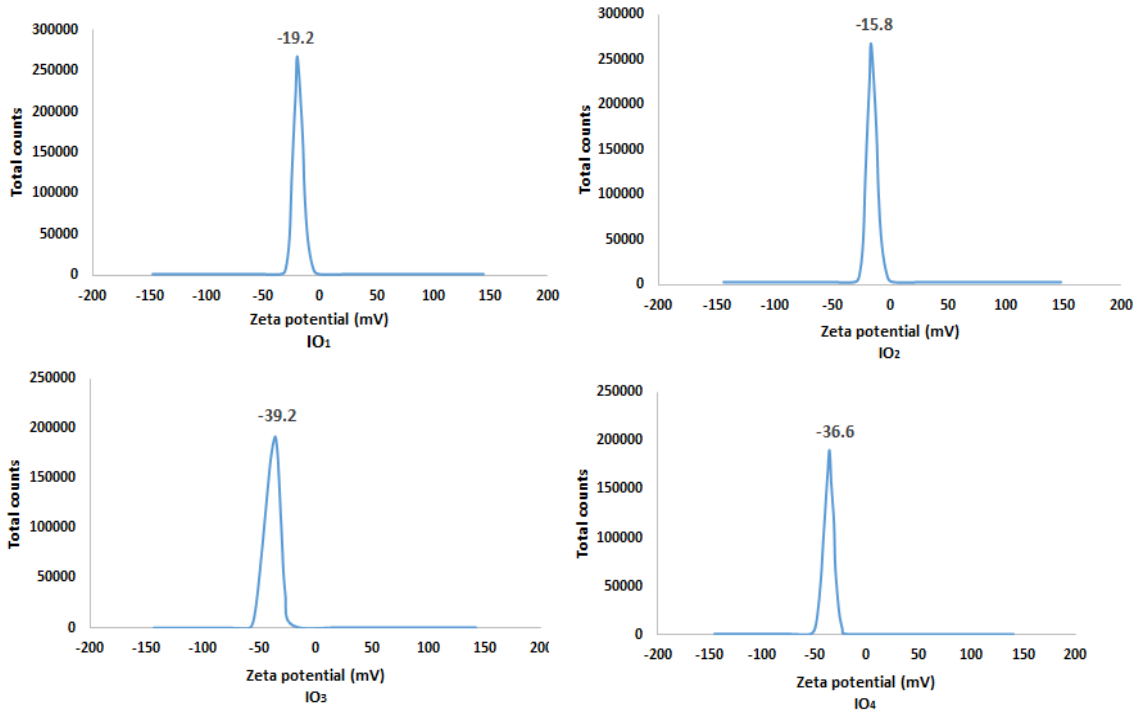


Fig. 3. The Zeta potential values of IONPs samples.

magnetite crystalline structure [22]. The recorded XRD patterns of four IONPs exhibited a great consistency without showing extra significant peaks. The interplanar spacings 'd_{hkl}' provided in Table 1 represent that all IONPs were produced in inverse cubic spinel structure of magnetite beyond 99% agreement with the reference. The highest intensity peak in all four IONPs corresponds to (311) plane from magnetite, implying that Fe_3O_4 considered as the major phase.

The full width at half maximum of the corresponding highest peak at 35° (311) and the crystallite size of four samples were calculated using Debye Scherer's formula (Table 1). The crystallinity of the synthesized magnetite phase of the samples was significantly governed by both the experimental variables; however, the effect of the synthesis atmosphere overweighed that of the alkaline reagents. In term of the alkaline reagent, the mild precipitator produced narrower peaks with higher intensity. Thereby, the IO_1 sample precipitated by NH_4OH under the N_2 atmosphere provided the narrowest peaks and thus the highest crystallite size (14 nm) among all the synthesized nanoparticles. The morphological investigation of the as-synthesized IONPs shown in Fig.5a-d indicated that all the nanoparticles were produced in spherical shapes, whereas the particle size range was different between varied samples where the

Table 1: Comparison of the XRD data of four IONPs samples.

	IO_1	IO_2	IO_3	IO_4
2 Theta (deg)	35.45	35.45	35.45	35.45
B (deg)	0.64	0.84	0.69	0.95
Crystallite Size (nm)	14	10	13	9
d spacing (Å) (311)	2.53	2.53	2.53	2.53

aerobic atmosphere resulted in higher agglomeration vulnerabilities. The produced agglomerates consisted of several nanoparticles and thus, the particle size distribution was difficult to precisely estimate. In general when the particle sizes are below 20 μm, the cohesive forces prevail the interparticle forces resulting in stronger tendency to particle agglomeration [23]. In contrast, the existence of N_2 in the atmosphere was significantly effective in the reducing the particles tendency to agglomeration through generation of repulsive forces among IO_1 and IO_3. In regard to the effect of alkaline solution, a slightly lower vulnerability to agglomeration was observed in the particles synthesized using NaOH solution, probably due to higher stabilities confirmed by the zeta potential values of the nanoparticles produced by this alkali, which consequently resulted in higher repulsive interparticle forces and enhanced dispersibility.

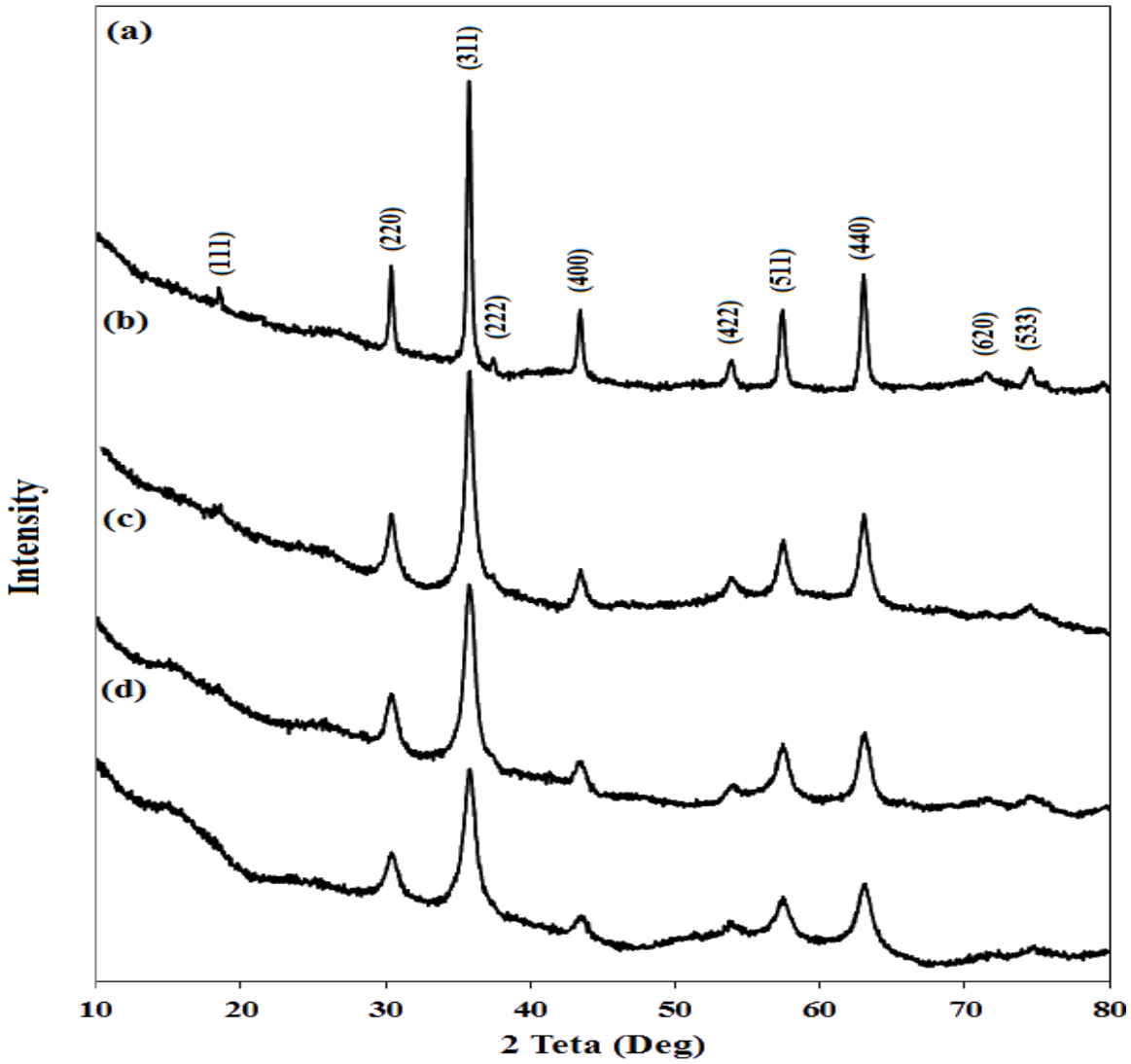


Fig. 4. XRD patterns and identified lattice indices of a) IO_1, b) IO_3, c) IO_2, and d) IO_4.

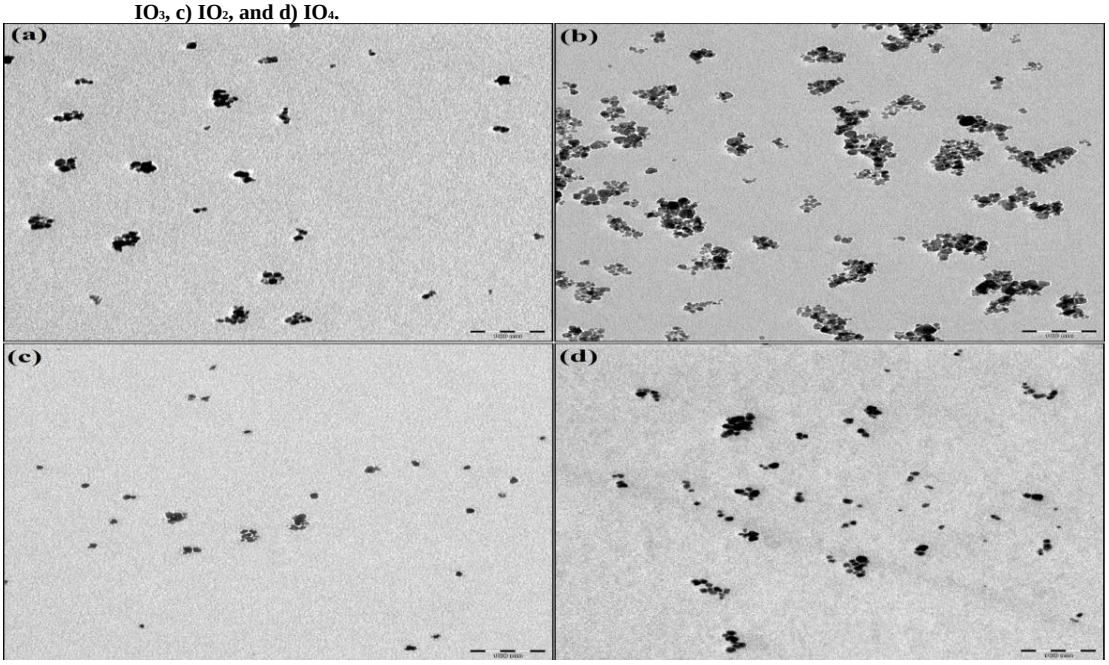


Fig. 5. Representative TEM images of a) IO_4, b) IO_2, c) IO_3, and d) IO_1.

In the other words, by addition of the strong alkaline reagent, the solubility of medium was swiftly attained which could overcome the condensational growing process, also called Ostwald ripening process [24, 25]. In contrast, precipitation by NH_4OH led to slightly smaller particle sizes (17±5 nm) compared to NaOH (20±5 nm), most likely due to a lower rate of particle formation in the weaker alkaline solution. Moreover, these average particle sizes of IONPs indicate that the sizes of as-synthesized nanoparticles are within the single domain region (<20 nm), implying superparamagnetic behavior which is in line with the findings of XRD analysis. Meanwhile, the determined particle sizes by TEM are bigger than the crystallite sizes determined using XRD pattern [26, 27]. The most obvious reason for this matter is that the XRD crystallite estimated by Scherrer–Debye relation is based on approximating the grain dimension, whereas the TEM particle size correlated with the entire particle which may be related to multiple grains [26].

The VSM magnetization curves of IONPs produced in varied experimental conditions at room temperature are illustrated in Fig.6 (a-d). The graphs clearly show that in all the samples, magnetization markedly enhanced with the increase of the magnetic field strength and saturated at above 0.4 T of AMF. Moreover, the hysteresis loops exhibited nearly zero remanence (Mr) and extremely low coercivity (Hc) values upon reduction of the AMF towards the opposite direction. These behaviours imply that all the pre-synthesized IONPs showed superparamagnetic characteristics with the magnetization curve in the form of sigmoidal shape like ferromagnetic materials, but without any loop [28] which are in good agreement with the particle size ranges observed in TEM analyses. However, comparison of the four varied IONPs revealed that those synthesized in $NH_4OH.N_2$ condition (Fig.6d) in overall could endow the highest Ms (59.62 $emu.g^{-1}$), the lowest Hc (4.99 G) as well as the lowest Mr (0.46 $emu.g^{-1}$) followed by IO_3 (Ms= 54.79 $emu.g^{-1}$, Hc= 6.07 G, Mr=0.64 $emu.g^{-1}$), IO_2 (Ms= 45.05 $emu.g^{-1}$, Hc= 7.70 G, Mr=0.48 $emu.g^{-1}$), and IO_4 (Ms= 43.42 $emu.g^{-1}$, Hc= 8.80 G, Mr= 0.48 $emu.g^{-1}$).

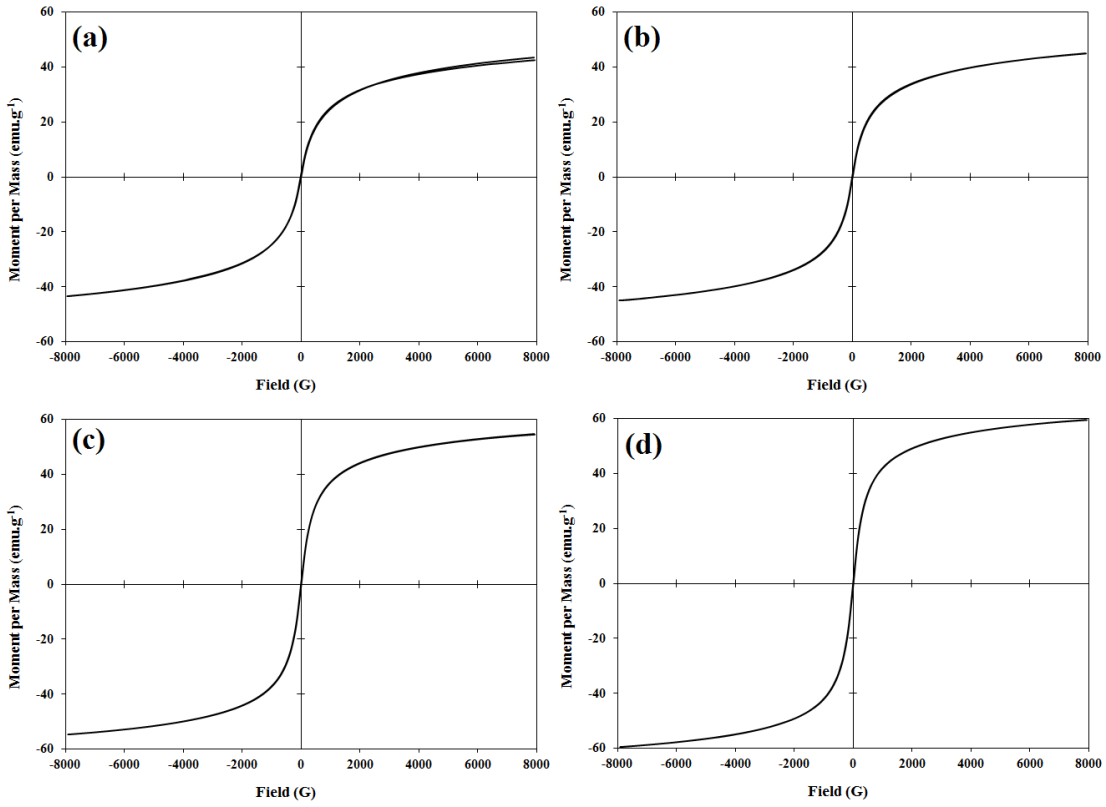


Fig. 6. Magnetic field-dependent magnetization curves at room temperature of a) IO_4, b) IO_2, c) IO_3, and d) IO_1.

It is important to note that all the IONPs exhibited the saturation magnetization values lower than that of bulk iron oxide with value of 92 $emu.g^{-1}$ [29]. This could be due to the presence of disordered magnetic spins at nanoparticles surfaces, which result in intrinsic reduction of Ms with increase of the magnetic field strength. In addition, the intensity of these disordered spins heightens while the particle size reduced due to the growth of the surface area-to-volume ratio [30, 31]. However, The Ms values of the four varied IONPs constantly raised with increase of the crystallite size as the magnetization generally relies on the ordered cores, domain size, and spin dynamics of the material surface [32, 33]. Thereby, the IONPs with highest crystallinity which were synthesized using mild alkaline reagent under the N_2

atmosphere (IO_1) provide enhanced alignment of their magnetic moments in the same direction of magnetic field. The existence of non-collinear spins at the crystals surface as well as the single domain nature of nanoparticles may also contribute to their enhanced Ms value [34, 35].

Treating cancerous tumors through MHT requires accurate calculation of saturation temperature as indicative of the magnitude of the generated heat within the tissues during exposure to AFM. A number of factors including both the physical and magnetic properties of the nanoparticles as well as the applied AMF parameters may affect the heating efficiency of IONPs. Hence, the achieved temperature distribution in the tissue could be regulated according to clinical requirements through alteration of the particles and AMF properties. However, in the clinical hyperthermia application, the AMF amplitude is limited by biological considerations as large field strength and frequencies may produce undue heating of the surrounding healthy tissues due to induced eddy currents. Hergt and Dutz [36] found that the multiplication of field amplitude and frequency must be limited to 5×10^9 $A.m^{-1}s^{-1}$ in order to prevent disorders in the patient's body. Therefore in order to perform an effective MHT, magnetic nanoparticles with high heating power are required to eradicate cancerous tumors with minimal dosages and AMF amplitudes.

As mentioned above, the IO_1 sample that synthesized by NH_4OH in N_2 atmosphere endowed the greatest crystallinity followed by highest net magnetization with reasonable stability and dispersion, thereby it was chosen as the optimal magnetic nanoagent to be examined for the induction heating examinations. The hyperthermic performance of such sample was quantified as heating power (SAR value) which determined by exposing the solutions containing IONPs to an external AMF and then recording the temperature variation as a function of time. The heating curves of five varied concentrations of IO_1 from 1 to 5 $mg.ml^{-1}$ with heating time up to 5400s in the varied magnetic field strength are illustrated in Fig.7a-e.

In all the thermal graphs, the temperature raised significantly over time under exposure to AMF fields with different amplitudes. The temperature rise in each graph was then moderated until reaching a maximum value known as saturation temperature.

The necessitous amount of saturation temperature to kill the malignant tissues is around 42°C whereas the temperature must also be

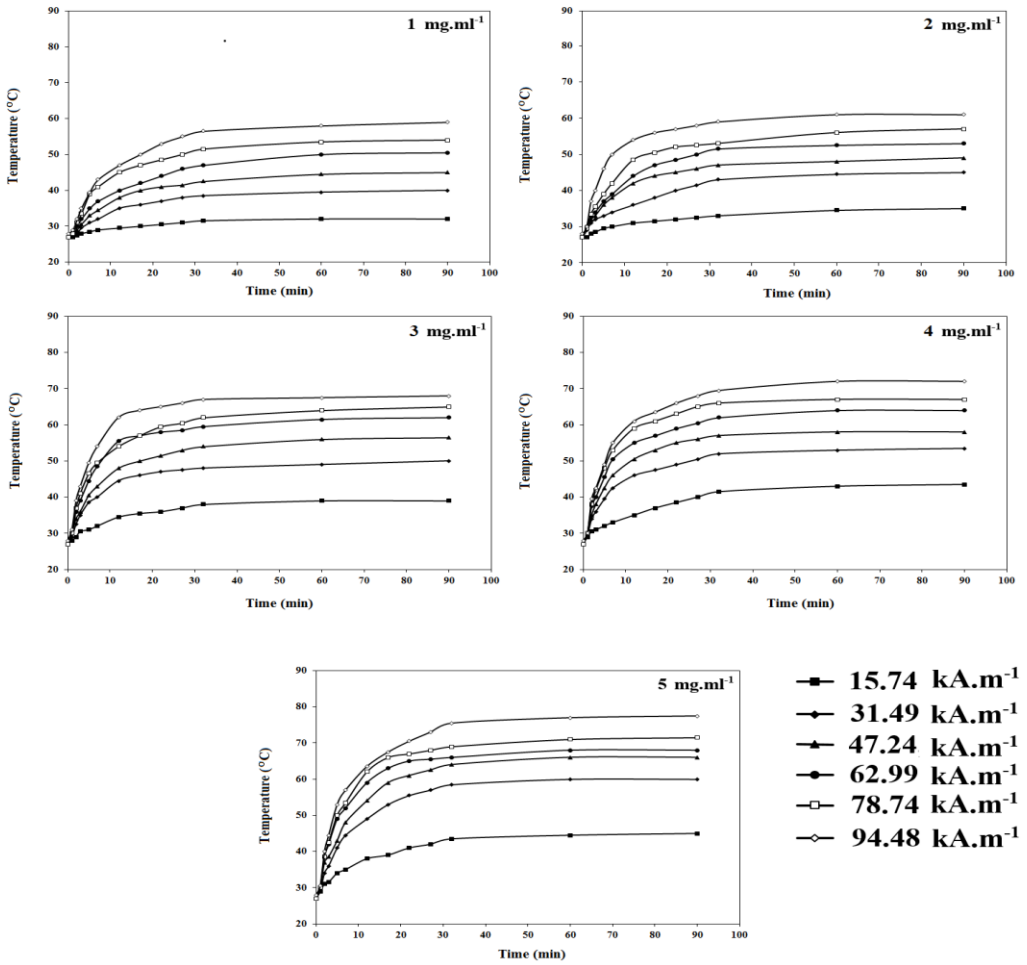


Fig. 7. The hyperthermia curves obtained for the IO_1 nanoparticles with varied concentrations in aqueous environments.

maintained below 46°C in order to protect normal tissues from undue heating. Taken into account that, when the induction heating experiments are performed in aqueous medium, the saturation temperature is restricted to the boiling point of the medium (i.e., 100°C) [37]. It is clearly observed from the Fig.7 that the temperature rise for the higher concentrations of IONPs is remarkably faster derived from the temperature dependency towards nanoparticles concentration [38]. The five varied concentrations of IO_1 become saturated at temperature of 45°C (1 $mg.ml^{-1}$), 45°C (2 $mg.ml^{-1}$), 50°C (3 $mg.ml^{-1}$), 43.5°C (4 $mg.ml^{-1}$) and 45°C (5 $mg.ml^{-1}$) in the presence of AMF with amplitude of 47.24, 31.49, 31.49, 15.74, and 15.74 $kA.m^{-1}$, respectively. These saturated results imply that IO_1 with low concentration either 1 $mg.ml^{-1}$ or 2 $mg.ml^{-1}$ at relatively low magnetic strengths of 47.24, 31.49 $kA.m^{-1}$ are desirable for MHT; however, by the consideration of the biological limit of physical parameters of AMF, only IO_1 with 2 $mg.ml^{-1}$ concentration may satisfy the hyperthermia condition. The heating capability of IONPs in destroying malignant tumors is considered as another essential parameter in MHT which could be determined from the induction heating curves (Fig.7a-e). Accordingly, the SAR values of IO_1 nanoparticles with five varied concentrations at different magnetic amplitudes were calculated based on the heating curves and provided in Table 2. In general, the SAR value of the superparamagnetic nanoparticles rises by increasing the magnetic field parameters, either the frequency or the amplitude or even both throughout the measurements [39]. Therefore, by increasing the field strength from 15.74 to 94.48 $kA.m^{-1}$, the SAR values enhanced greatly for all concentrations due to heating loss mechanisms of IONPs.

Concentration ($mg.ml^{-1}$)	Amplitude ($kA.m^{-1}$)	Frequency (KHz)	SAR ($W.g_{Fe}$)	SAR ($W.g_{IONPs}$)	ILP_{Fe} ($nHm^2.kg^{-1}$)	ILP_{IONPs} ($nHm^2.kg^{-1}$)	TH (°C)
1	15.74	326	43.54	31.35	0.539	0.388	32
	31.49	318	106.25	76.50	0.336	0.242	40
	47.24	313	157.34	113.29	0.225	0.162	45
	62.99	312	210.18	151.33	0.169	0.122	50.5
	78.74	311	291.47	209.86	0.151	0.108	54
	94.48	310	316.43	227.84	0.114	0.082	59
2	15.74	326	38.82	27.17	0.481	0.336	35
	31.49	318	99.44	69.61	0.315	0.221	45
	47.24	313	124.23	86.97	0.177	0.124	49
	62.99	312	161.56	113.10	0.131	0.091	53
	78.74	311	186.64	130.66	0.096	0.067	57
	94.48	310	248.76	174.15	0.089	0.062	61
3	15.74	326	33.05	23.13	0.409	0.286	39
	31.49	318	91.19	63.84	0.289	0.202	50
	47.24	313	116.08	81.26	0.166	0.116	56.5
	62.99	312	149.33	104.54	0.125	0.084	62
	78.74	311	165.85	116.11	0.086	0.060	65
	94.48	310	199.10	139.39	0.071	0.050	68
4	15.74	326	29.87	20.91	0.369	0.258	43.5
	31.49	318	87.07	60.96	0.276	0.193	53.5
	47.24	313	99.46	70.79	0.142	0.101	58
	62.99	312	130.68	91.49	0.105	0.073	64
	78.74	311	136.80	95.78	0.071	0.049	67
	94.48	310	155.47	108.85	0.056	0.039	72
5	15.74	326	26.72	19.24	0.331	0.238	45
	31.49	318	67.73	48.77	0.214	0.154	60
	47.24	313	96.77	68.6	0.138	0.098	66
	62.99	312	106.41	76.63	0.085	0.061	68
	78.74	311	111.29	80.15	0.057	0.044	71.5
	94.48	310	125.81	90.60	0.045	0.032	77.5

However, the reduction in SAR value observed with increasing the concentration can be resulted from

dipolar interactions among IONPs. Two main reasons bring about the reduction in the trend of SAR value; the magnetic susceptibility of IONPs reduces with increase of their concentration, which in turn increases the dipolar interactions and make them remarkably stable against the orientation of AMF. Secondly, the heating loss mechanisms are declined when the interaction among nanoparticles is increased, giving rise to IONPs relaxation and decrease of their heating performances [40]. In other words, the dipole-dipole interactions in concentrated IONPs are stronger, affecting the MHT efficiency through reducing the heating loss dynamics of the magnetic moments and/or increasing the magnetic anisotropy.

The main governing mechanism in heat loss dissipation of superparamagnetics is related to Néel and Brownian relaxation losses, described by Rosensweig in the Linear Response Theory (LRT) [41]. The magnetization results from VSM graphs implied that IONPs are superparamagnetic which followed by heating relaxation losses. According to LRT, a purely "magnetic" Néel relaxation occurs due to the rotation of magnetic moments within the crystal. In a "viscous" Brownian relaxation, the magnetic moments inside the crystal axis align with the AMF and the nanoparticles rotate as well by following the field.

The Brownian relaxation time, τ_B, as well as Néel relaxation time, τ_N, for spherical particles are given by the following relationships [41]:

$$\tau_B = \frac{3VH\eta}{kBT} \quad (5)$$

$$\tau_N = \tau_0 e^{\frac{KV}{KT}} \quad (6)$$

where V_H is the hydrodynamic particle volume, η represents the fluid viscosity, k denotes the Boltzmann constant (1.38×10^{-23} J.K^{-1}). The T, τ_0, V, and K also represent the absolute temperature (K), time constant, particle volume, and magnetocrystalline anisotropy, respectively. The Néel relaxation time depends on the anisotropy and volume of magnetic nanoparticles, whereas the viscose relaxation is associated with the Brownian relaxation time and relies on the medium viscosity and the hydrodynamic diameter.

The spherical IO_1 with 14 nm particle size is in accordance to the magnetite sample model of Rosensweig [41] as well as Deatsch and Evans [42] with the same particle size. Hence, in an aqueous medium (K= 25 kJ.m^{-3}, η = 8.9×10^{-4} Pa s) and based on their presented relation time graph as a function of particle size, the τ_N value is approximately 10 times lower than τ_B, thus Néel relaxation time occurs much faster and considered as the governing heating mechanism. The SAR values of IO_1 reduced with increase of the concentration and thus, the highest and lowest SAR belonged to 1 and 5 mg.ml^{-1} concentration with values of 316.43 and 125.81 W.g^{-1}, respectively. The reason behind the reduction of heating power of IONPs is probably the dipole-dipole interactions among the magnetic nanoparticles. As a matter of the fact, increase of the nanoparticle concentration results in declined separation of the nanoparticles, leading to enhancement of the dipolar interactions and decrease of the domain heating loss "Néel relaxation time", which subsequently reduce the generated heat by the magnetic nanoparticles [38, 42, 43].

CONCLUSION

The obtained results indicated the significant contribution of alkaline reagents and synthesis atmosphere on chemical, morphological, and magnetic characteristics of the produced nanoparticles, where synthesis atmosphere played a more significant role compared to the alkaline reagent type in determining the particles crystallinity and magnetization characteristics where using NH_4OH resulted in lower rates of particle formation and thus, higher crystallization and improved magnetic behavior. On the other hand, when NaOH was used as the precipitating agent, higher zeta potential values and thus slightly lower aggregation tendencies were achieved. However, this effect was negligible when synthesis was carried out under the anaerobic atmosphere. Therefore, in order to obtain nanoparticles with higher crystallinity and enhanced magnetic behavior as well as sufficient stability in aqueous medium, the synthesis process is recommended to be carried out under anaerobic atmosphere using NH_4OH as the precipitating reagent. The investigation on the induction heating of such optimal IONPs indicated that the SAR value was dependent on the AMF strength as well as the IONPs concentration in the ferrofluid. The lowest SAR values belonged to the highest IONPs concentrations in the whole range of field amplitudes due to the dipolar interaction among nanoparticles, which led to reduced heating loss via Néel relaxation mechanism.

ACKNOWLEDGEMENT

The authors appreciate the University of Malaya for financial support through the UMRG project number RP042A-17AET.

REFERENCES

[1] C. Iacovita, A. Florea, R. Dudric, E. Pall, A. I. Moldovan, R. Tetean, R. Stiufiuc, and C. M. Lucaciu, "Small versus Large Iron Oxide Magnetic Nanoparticles: Hyperthermia and Cell Uptake Properties," Molecules, vol. 21, no. 10, pp. 2016.

[2] J. Yang, M. Pan, R. Shi, L. Yang, J. Wang, X. Kong, W. Yang, D. Wang, and Z. Zhou, Novel Fe3O4 hollow microspheres: Nontemplate hydrothermal synthesis, superparamagnetism and biocompatibility. Vol. 9. 2017. 109-117.

[3] M. A. Gonzalez-Fernandez, T. E. Torres, M. Andrés-Vergés, R. Costo, P. de la Presa, C. J. Serna, M. P. Morales, C. Marquina, M. R. Ibarra, and G. F. Goya, "Magnetic nanoparticles for power absorption: Optimizing size, shape and magnetic properties," Journal of Solid State Chemistry, vol. 182, no. 10, pp. 2779-2784, 2009.

[4] L. Yu, J. Liu, K. Wu, T. Klein, Y. Jiang, and J.-P. Wang, "Evaluation of Hyperthermia of Magnetic Nanoparticles by Dehydrating DNA," Scientific Reports, vol. 4, no. pp. 7216, 2014.

[5] J. Verma, S. Lal, and C. J. F. Van Noorden, "Nanoparticles for hyperthermic therapy: synthesis strategies and applications in glioblastoma," International Journal of Nanomedicine, vol. 9, no. pp. 2863-2877, 2014.

[6] S. V. Spirou, S. A. Costa Lima, P. Bouziotis, S. Vranjes-Djuric, E. Efthimiadou, A. Laurenzana, A. I. Barbosa, I. Garcia-Alonso, C. Jones, D. Jankovic, and O. L. Gobbo, "Recommendations for In Vitro and In Vivo Testing of Magnetic Nanoparticle Hyperthermia Combined with Radiation Therapy," Nanomaterials (Basel), vol. 8, no. 5, pp. 2018.

[7] Z. Hedayatnasab, F. Abnisa, and W. M. A. W. Daud, "Review on magnetic nanoparticles for magnetic nanofluid hyperthermia application," Materials & Design, vol. 123, no. pp. 174-196, 2017.

[8] M. C. Mascolo, Y. Pei, and T. A. Ring, "Room Temperature Co-Precipitation Synthesis of Magnetite Nanoparticles in a Large pH Window with Different Bases," Materials, vol. 6, no. 12, pp. 5549-5567, 2013.

[9] V. V. Kharton, A. L. Shaula, F. M. M. Snijkers, J. F. C. Cooymans, J. J. Luyten, A. A. Yaremchenko, A. A. Valente, E. V. Tsipis, J. R. Frade, F. M. B. Marques, and J. Rocha, "Processing, stability and oxygen permeability of Sr(Fe, Al)O3-based ceramic membranes," Journal of Membrane Science, vol. 252, no. 1, pp. 215-225, 2005.

[10] D. Dorniani, M. Z. B. Hussein, A. U. Kura, S. Fakurazi, A. H. Shaari, and Z. Ahmad, "Preparation of Fe3O4 magnetic nanoparticles coated with gallic acid for drug delivery," International Journal of Nanomedicine, vol. 7, no. pp. 5745-5756, 2012.

[11] M. P. Kingsley, P. B. Desai, and A. K. Srivastava, "Simultaneous electro-catalytic oxidative determination of ascorbic acid and folic acid using Fe3O4 nanoparticles modified carbon paste electrode," Journal of Electroanalytical Chemistry, vol. 741, no. pp. 71-79, 2015.

[12] N. Kumam, L. P. Singh, S. K. Srivastava, and N. R. Singh, "Photoluminescence properties of Eu3+ doped BaF2 nanomaterials and BaF2:3Eu/Fe3O4 nanocomposite for hyperthermia application," Journal of Luminescence, vol. 203, no. pp. 59-66, 2018.

[13] P. B. Shete, R. M. Patil, N. D. Thorat, A. Prasad, R. S. Ningthoujam, S. J. Ghosh, and S. H. Pawar, "Magnetic chitosan nanocomposite for hyperthermia therapy application: Preparation, characterization and in vitro experiments," Applied Surface Science, vol. 288, no. pp. 149-157, 2014.

[14] N. P. Singh, L. P. Singh, N. R. Singh, and S. K. Srivastava, "Photoluminescence properties of SrF2:3Tb@BaF2 nanoparticles and improved hyperthermia temperature achieved by core-shell nanohybrid SrF2:3Tb@BaF2/Fe3O4 materials," Colloid and Polymer Science, vol. 296, no. 2, pp. 355-365, 2018.

[15] H. Chiriac, T. Petreus, E. Carasevici, L. Labusca, D.-D. Herea, C. Danceanu, and N. Lupu, "In vitro cytotoxicity of fe–cr–nb–b magnetic nanoparticles under high frequency electromagnetic field," Journal of Magnetism and Magnetic Materials, vol. 380, no. pp. 13-19, 2015.

[16] V. M. Khot, A. B. Salunkhe, N. D. Thorat, R. S. Ningthoujam, and S. H. Pawar, "Induction heating studies of dextran coated mgfe2o4 nanoparticles for magnetic hyperthermia," Dalton Trans, vol. 42, no. 4, pp. 1249-58, 2013.

[17] G. Kandasamy, A. Sudame, P. Bhati, A. Chakrabarty, S. N. Kale, and D. Maity, "Systematic magnetic fluid hyperthermia studies of carboxyl functionalized hydrophilic superparamagnetic iron oxide nanoparticles based ferrofluids," Journal of Colloid and Interface Science, vol. 514, no. pp. 534-543, 2018.

[18] M. Srivastava, S. K. Alla, S. S. Meena, N. Gupta, R. K. Mandal, and N. K. Prasad, "ZnxFe3−xO4 ($0.01 \leq x \leq 0.8$) nanoparticles for controlled magnetic hyperthermia application," New Journal of Chemistry, vol. 42, no. 9, pp. 7144-7153, 2018.

[19] T. Ahn, J. H. Kim, H.-M. Yang, J. W. Lee, and J.-D. Kim, "Formation pathways of magnetite nanoparticles by coprecipitation method," The Journal of Physical Chemistry C, vol. 116, no. 10, pp. 6069-6076, 2012.

[20] Y. Yin, Z. Hu, W. Du, F. Ai, R. Ji, J. L. Gardea-Torresdey, and H. Guo, "Elevated CO2 levels increase the toxicity of ZnO nanoparticles to goldfish (Carassius auratus) in a water-sediment ecosystem," Journal of Hazardous Materials, vol. 327, no. pp. 64-70, 2017.

[21] A. Ali, H. Zafar, M. Zia, I. ul Haq, A. R. Phull, J. S. Ali, and A. Hussain, "Synthesis, characterization, applications, and challenges of iron oxide nanoparticles," Nanotechnology, Science and Applications, vol. 9, no. pp. 49-67, 2016.

[22] H. Unterweger, L. Dézsi, J. Matuszak, C. Janko, M. Poettler, J. Jordan, T. Bäuerle, J. Szebeni, T. Fey, A. R. Boccaccini, C. Alexiou, and I. Cicha, "Dextran-coated superparamagnetic iron oxide nanoparticles for magnetic resonance imaging: evaluation of size-dependent imaging properties, storage stability and safety," International Journal of Nanomedicine, vol. 13, no. pp. 1899-1915, 2018.

[23] K. S. Hayden, K. Park, and J. S. Curtis, "Effect of particle characteristics on particle pickup velocity," Powder Technology, vol. 131, no. 1, pp. 7-14, 2003.

[24] G. Cao and Y. Wang, Physical Chemistry of Solid Surfaces, in Nanostructures and Nanomaterials. 2011, WORLD SCIENTIFIC. p. 19-60.

[25] T. Q. Bui, S. N.-C. Ton, A. T. Duong, and H. T. Tran, "Size-dependent magnetic responsiveness of magnetite nanoparticles synthesised by co-precipitation and solvothermal methods," Journal of Science: Advanced Materials and Devices, vol. 3, no. 1, pp. 107-112, 2018.

[26] A. Itztani Cervantes-Macías, C. A. Huerta Aguilar, and P. Thangarasu, ZnO–Fe3O4–Au Hybrid Composites for Thioanisole Oxidation Under Visible Light: Experimental and Theoretical Studies. 2017.

[27] A. I. Prasad, A. K. Parchur, R. R. Juluri, N. Jadhav, B. N. Pandey, R. S. Ningthoujam, and R. K. Vatsa, "Bi-functional properties of Fe3O4@YPO4:Eu hybrid nanoparticles: hyperthermia application," Dalton Transactions, vol. 42, no. 14, pp. 4885-4896, 2013.

[28] C. Schweiger, R. Hartmann, F. Zhang, W. J. Parak, T. H. Kissel, and P. Rivera_Gil, "Quantification of the internalization patterns of superparamagnetic iron oxide nanoparticles with opposite charge," Journal of Nanobiotechnology, vol. 10, no. 1, pp. 28, 2012.

[29] L. Liu, Z. He, Y. Zhao, J. Sun, and G. Tong, "Modulation of the composition and surface morphology of expanded graphite/Fe/Fe3O4 composites for plasmon resonance-enhanced microwave absorption," Journal of Alloys and Compounds, vol. 765, no. pp. 1218-1227, 2018.

[30] M. A and K. C, "Low Curie-transition temperature and superparamagnetic nature of Fe3O4 nanoparticles prepared by colloidal nanocrystal synthesis," Materials Chemistry and Physics, vol. 192, no. pp. 235-243, 2017.

[31] C. Caizer, Nanoparticle Size Effect on Some Magnetic Properties, in Handbook of Nanoparticles, M. Aliofkhazraei, Editor. 2015, Springer International Publishing: Cham. p. 1-38.

[32] R. B. Kamble, V. Varade, K. P. Ramesh, and V. Prasad, "Domain size correlated magnetic properties and electrical impedance of size dependent nickel ferrite nanoparticles," AIP Advances, vol. 5, no. 1, pp. 017119, 2015.

[33] A. K. Agustina, J. Utomo, E. Suharyadi, T. Kato, and S. Iwata, "Effect of Synthesis Parameters on Crystals Structures and Magnetic Properties of Cobalt Nickel Ferrite Nanoparticles," IOP Conference Series: Materials Science and Engineering, vol. 367, no. 1, pp. 012006, 2018.

[34] L. E. Wenger, G. M. Tsoi, P. P. Vaishnava, U. Senaratne, E. C. Buc, R. Naik, and V. M. Naik, "Magnetic Properties ofγ-Fe2O3Nanoparticles Precipitated in Alginate Hydrogels," IEEE Transactions on Magnetics, vol. 44, no. 11, pp. 2760-2763, 2008.

[35] N. M. Deraz, "Size and crystallinity-dependent magnetic properties of copper ferrite nano-particles," Journal of Alloys and Compounds, vol. 501, no. 2, pp. 317-325, 2010.

[36] R. Hergt and S. Dutz, "Magnetic particle hyperthermia—biophysical limitations of a visionary tumour therapy," Journal of Magnetism and Magnetic Materials, vol. 311, no. 1, pp. 187-192, 2007.

[37] V. Nica, H. M. Sauer, J. Embs, and R. Hempelmann, "Calorimetric method for the determination of Curie temperatures of magnetic nanoparticles in dispersion," Journal of Physics: Condensed Matter, vol. 20, no. 20, pp. 204115, 2008.

[38] Y. Iqbal, H. Bae, I. Rhee, and S. Hong, "Magnetic heating of silica-coated manganese ferrite nanoparticles," Journal of Magnetism and Magnetic Materials, vol. 409, no. pp. 80-86, 2016.

[39] P. Guardia, R. Di Corato, L. Lartigue, C. Wilhelm, A. Espinosa, M. Garcia-Hernandez, F. Gazeau, L. Manna, and T. Pellegrino, "Water-Soluble Iron Oxide Nanocubes with High Values of Specific Absorption Rate for Cancer Cell Hyperthermia Treatment," ACS Nano, vol. 6, no. 4, pp. 3080-3091, 2012.

[40] A. Urtizberea, E. Natividad, A. Arizaga, M. Castro, and A. Mediano, "Specific Absorption Rates and Magnetic Properties of Ferrofluids with Interaction Effects at Low Concentrations," The Journal of Physical Chemistry C, vol. 114, no. 11, pp. 4916-4922, 2010.

[41] R. E. Rosensweig, "Heating magnetic fluid with alternating magnetic field," Journal of Magnetism and Magnetic Materials, vol. 252, no. pp. 370-374, 2002.

[42] A. E. Deatsch and B. A. Evans, "Heating efficiency in magnetic nanoparticle hyperthermia," Journal of Magnetism and Magnetic Materials, vol. 354, no. pp. 163-172, 2014.

[43] A. Ahmad, H. Bae, and I. J. J. o. t. K. P. S. Rhee, "Cube-Shaped Cetyltrimethyl Ammonium Bromide-Coated Nickel Ferrite Nanoparticles for Hyperthermia Applications," vol. 73, no. 1, pp. 125-129, 2018.

★★★